Complex flow around a bubble rising in a non-Newtonian fluid

Xavier Frank and Huai Z. Li*

Laboratoire des Sciences du Génie Chimique (CNRS, UPR 6811), ENSIC-INPL, 1, rue Grandville, BP 451, 54001 Nancy Cedex, France

(Received 31 March 2004; revised manuscript received 18 January 2005; published 22 March 2005)

Our experimental investigation by both particle image velocimetry and birefringence modulation method shows very complex flow features around a bubble rising in a non-Newtonian fluid. We model this two-phase flow by coupling the free-energy-based lattice Boltzmann scheme and the fluid rheology in the framework of the sixth-order Maxwell model with shear thinning effects. A Newtonian low viscosity drop is used to simulate the rising bubble. Numerical results including noticeably negative wake behind the bubble, stress field, as well as the bubble's teardrop shape are obtained, and compare satisfactorily with our experiments.

DOI: 10.1103/PhysRevE.71.036309 PACS number(s): 47.50.+d, 47.55.Dz

I. INTRODUCTION

Bubble dynamics in non-Newtonian fluids is of great academic interest and industrial relevance in such diverse domains as polymer devolatilization, volcanic eruption, decompression sickness, fermentation, glass manufacture, wastewater treatment, and metallurgy. Since the pioneer works [1,2], considerable efforts have been directed at elucidating a number of particular phenomena not observed in Newtonian fluids such as the negative wake behind a bubble revealed by the laser Doppler anemometer (LDA) measurements at a point in fluid [3] and the memory effects in stress relaxation [4,5]. Recently, the lattice Boltzmann (LB) method as a mesoscopic approach to the simulation of fluid dynamics has been shown to give convincing results for Newtonian one-component flows [6]. It has also been applied to Newtonian two-phase flows with promising perspectives [7–9]. However, there are still few studies towards the inclusion of viscoelastic properties in the lattice Boltzmann method even for one-component flows [10–12]. Therefore it is our aim here to elaborate a suitable lattice Boltzmann model for a gas bubble rising in non-Newtonian fluids.

II. EXPERIMENT

Experiments were conducted in a Plexiglas cylindrical column of 0.3 m diameter surrounded by a square duct and filled with a solution of 0.50 wt % polyacrylamide (PAAm, average molecular weight of 6.96×10^6 g mol^{-1}) in water to a depth of 0.5 m. This fluid was shear thinning and viscoelastic. Air bubbles were individually generated by a computer-controlled electronic valve through a submerged orifice of 1 mm diameter at the bottom section. The bubble shape was always axisymmetric for considered volumes up to 1100 mm^3 [13,14]. Both the experimental and theoretical results presented below correspond to a steady flow where the bubble's terminal rise velocity was reached.

A particle image velocimetry (PIV) three-dimensional (3D) system with two YAG lasers and two cameras (Dantec Dynamics) was used to measure the fluid flow field around a bubble with the help of fluorescent seeding particles. Owing to the axisymmetry of the bubble, our measurements were performed for two-dimensional (2D) flow fields in a plane containing the axis of symmetry of the bubble. The flow field around a bubble in the PAAm solution has a very peculiar shape (Fig. 1), compared with the one in a viscous Newtonian fluid. In the central wake, the movement of the fluid is surprisingly downward to form a so called negative wake. A cone of upward flow surrounds this negative wake. This zone begins on the sides of the bubble and is developed backward.

Under shearing, a polymer solution may exhibit birefringent behavior as a consequence of stretching of polymeric chains. To provide evidence of the stresses around bubbles in our fluid, flow birefringence measurements were performed based on polarization modulation method. This method provides mainly useful information about the localization of stresses. In Fig. 2, typical examples of butterflylike spatial distribution of stresses around a bubble are shown in 0.50% PAAm solution for a bubble volume of respectively 80 and 190 mm^3. White zones illustrate the existence of axisymmetric stresses, in front of the bubble due to the fluid compression and especially behind the bubble at the border of the negative wake due to the relative movement of fluid, while black zones owing to the extinction of the polarized light characterize the absence of stress.

III. SIMULATION METHOD

To simulate a bubble rising in a non-Newtonian fluid, we chose the free-energy-based model developed initially in Oxford [15,16] for a binary fluid. Macroscopic quantities ρ, $\vec{u}$ and $\Delta\rho$ are deduced from functions f_i and g_i [15]. The bubble was assimilated as a drop where $\Delta\rho>0$. If external forces are imposed to the fluid, these forces result in an acceleration $\vec{a}$. Functions f_i obey the lattice Boltzmann equation (1) and (2), where the parameter t_f is a dimensionless time, linked to fluid's kinematic viscosity as $\nu_{LB}=t_f\delta t c_s^2$, t_g is another dimensionless time parameter that is chosen equal to 1 according to the literature [8,17],

*Electronic address: li@ensic.inpl-nancy.fr

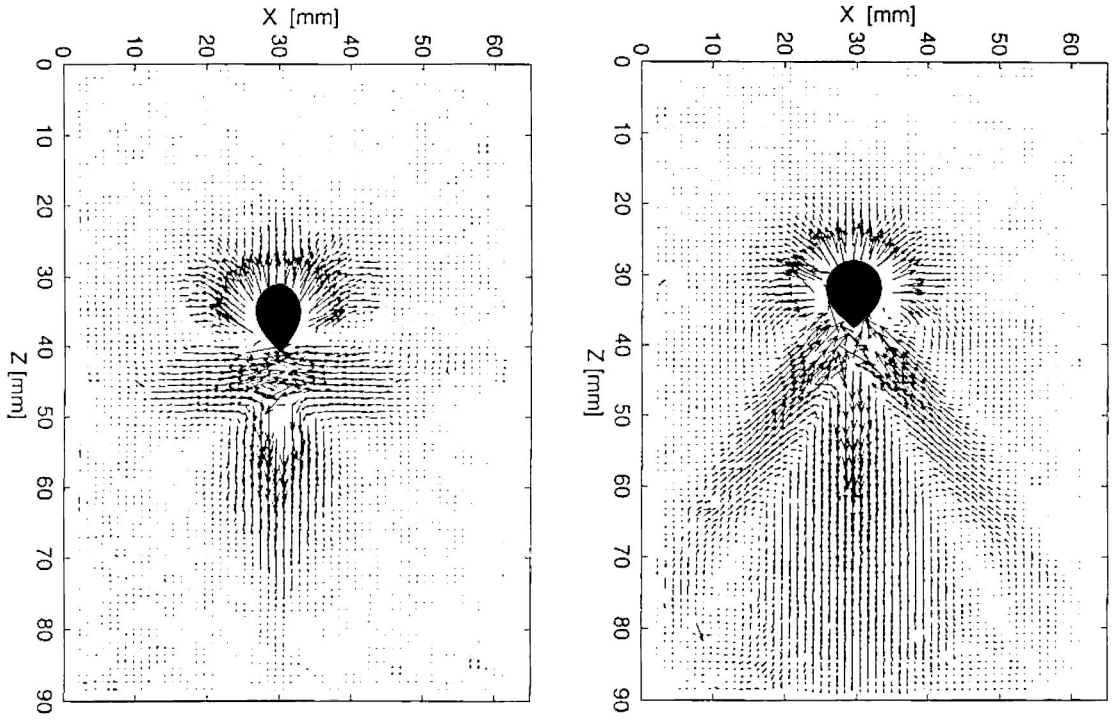

FIG. 1. Flow field obtained by PIV measurements around a bubble in 0.50% PAAm solution. The bubble volume $V_0 = 80$ mm^3 on the left; $V_0 = 190$ mm^3 on the right. The real bubble shape is artificially added.

$$f_i(\vec{r} + \delta t\vec{c}_i, t + \delta t) - f_i(\vec{r}, t) = -\frac{[f_i(\vec{r}, t) - f_i^{eq}(\vec{r}, t)]}{t_f} + \frac{\vec{a} \cdot (\vec{c}_i - \vec{u})}{c_s^2} f_i^{eq}(\vec{r}, t), \quad (1)$$

$$g_i(\vec{r} + \delta t\vec{c}_i, t + \delta t) - g_i(\vec{r}, t) = -\frac{[g_i(\vec{r}, t) - g_i^{eq}(\vec{r}, t)]}{t_g}. \quad (2)$$

The functions f_i^{eq} and g_i^{eq} are equilibrium ones. Well-known thermodynamic quantities used to compute them, pressure tensor $P_{\alpha\beta}$ and chemical potential difference $\Delta\mu$, are derived from conserved quantities [16]. Interfacial tension is controlled by the parameter κ, involved in $P_{\alpha\beta}$ and $\Delta\mu$ definition; we chose $\kappa = 0.05$, a classical value for air-aqueous systems.

IV. RHEOLOGICAL MODEL

A suitable rheological model is required to allow both the description of main viscoelasticity features. We used a modified sixth-order Maxwell fluid. The model finds its physical

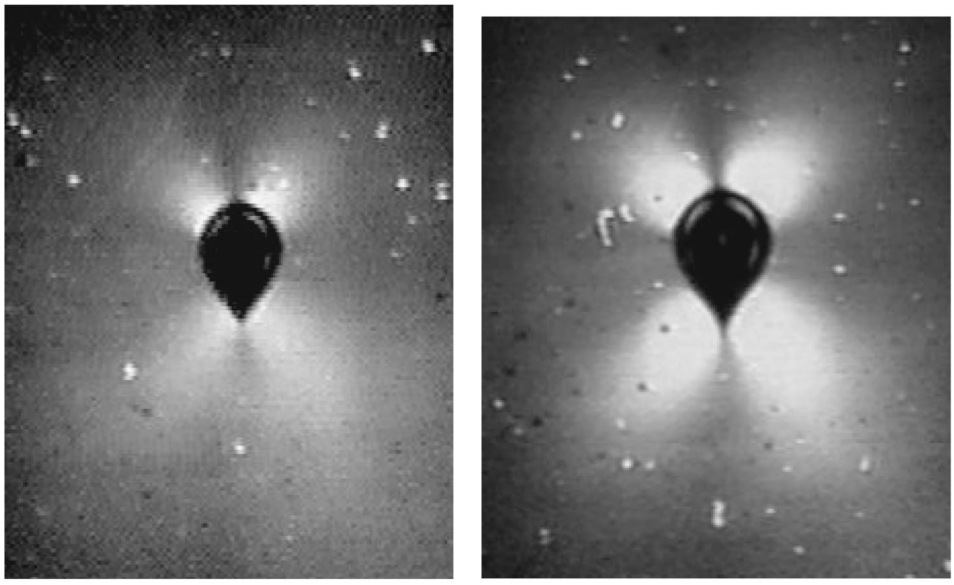

FIG. 2. Stress around a bubble rising in 0.50% PAAm solution visualized by birefringence measurement. On the left: bubble volume 80 mm^3; on the right: bubble volume 190 mm^3.

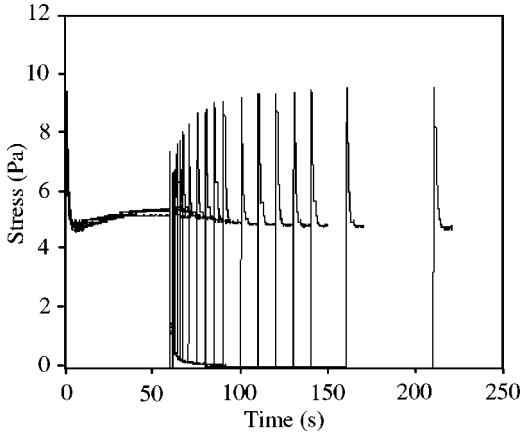

FIG. 3. Successive relaxation experiments, time delay, respectively: 1, 2, 3, 5, 7, 10, 15, 20, 25, 30, 40, 50, 60, 70, 90, 120, 150 s.

justification by our previous studies concerning the linear superposition of accumulated stresses in fluid due to consecutive passages of a regular train of identical bubbles [4,5,14]. We then used a linear viscoelasticity model of Maxwell composed of six stress tensors whose sum leads to the total stress tensor (3)–(5), where (G_k, λ_k) are the coefficients of the sixth-order Maxwell fluid, obtained experimentally by rheological characterization,

$$\sum_{k=1}^{6} \tau_{i,j}^{k} = \tau_{i,j}, \tag{3}$$

$$\frac{\partial \tau_{i,j}^{k}}{\partial t} = G_k D_{i,j} - \frac{1}{\lambda_k'} \tau_{i,j}^{k}, \tag{4}$$

$$D_{i,j} = \partial_i u_j + \partial_j u_i. \tag{5}$$

In order to satisfy the dynamical behavior experimentally observed in successive relaxation tests (Fig. 3), we introduce a physical quantity $\phi(\vec{r},t)$ that is a phenomenological parameter of fluid's viscosity evolution, obeying a relaxation equation (8) and (9),

$$\lambda_k' = \lambda_k \frac{\eta(\phi)}{\sum_k \lambda_k G_k}, \tag{6}$$

$$\frac{\eta - \eta_\infty}{\eta_0 - \eta_\infty} = [1 + (\lambda\phi)^2]^{(n-1)/2}. \tag{7}$$

The quantity $I_D^{(2)}$ is the second invariant of the tensor $D_{i,j}$. Relaxation times λ_k' depend on ϕ (6) and (7) so that asymptotical viscosity reaches the correct value described by an experimentally fitted Carreau model (7),

$$\frac{\partial \phi}{\partial t} = -\frac{\phi - \sqrt{|I_D^{(2)}|}}{t_r}, \tag{8}$$

$$t_r = \frac{t_{r0}}{1 + \dfrac{\phi}{\phi_0}}. \tag{9}$$

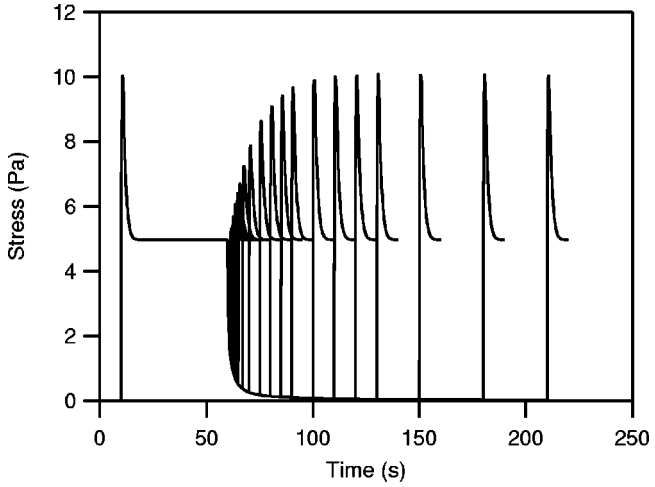

FIG. 4. Computation of the stress exhibited in same conditions as successive relaxation experiments.

To validate this model, we performed consecutive relaxation experiments. The fluid was sheared during 50 s followed by a time interval during which the fluid was remained at rest, another steady shearing was then imposed to the fluid with the same shear rate. The fluid's stress was monitored (Fig. 3). It is worth noting that the parameters G_k and λ_k and as well as that in the Carreau model were determined by the standard rheological characterization. Consecutive relaxation experiments allowed us only to choose $t_{r0} = 12$ s and $\phi_0 = 0.50\ \mathrm{s}^{-1}$, in comparison to the computation of the fluids stress response by Eqs. (3)–(7). As shown in Figs. 3 and 4, this model describes correctly the relaxation behavior, a central phenomena governing the passage of a bubble in fluid.

V. NUMERICAL RESULTS

We integrated the above numerical scheme by means of a classical D2Q9 lattice 200 nodes large and 400 nodes high, and solid walls for borders of the simulation box, to discretize the phase space. In order to implement the Newtonian behavior inside the drop, we let parameters (G_k, λ_k) depend on $\Delta\rho$ in such a way that inside the bubble, $G_k = 0$ and the tensors $\tau_{i,j}^k$ are forced to relax quickly as relaxation times λ_k are 100 times shorter than in the bulk liquid. As $c_{i\alpha}$ is the α component of the ith direction velocity $\vec{c}_i$ of the lattice, the total stress tensor $\tau_{i,j}$ is used as follows:

$$\sum_i f_i^{eq} c_{i\alpha} c_{i\beta} = \rho u_\alpha u_\beta + P_{\alpha\beta} - \tau_{\alpha\beta}. \tag{10}$$

As shown in Fig. 5, the flow field was successfully simulated: a central negative wake does appear behind the bubble and the upward flow has a cone shape surrounding this downward wake. With respect to the birefringence method, we plotted computed shear stresses around a bubble (Fig. 6). A butterflylike shape, mainly due to the strong velocity gradients located at the interface between the upward flow and

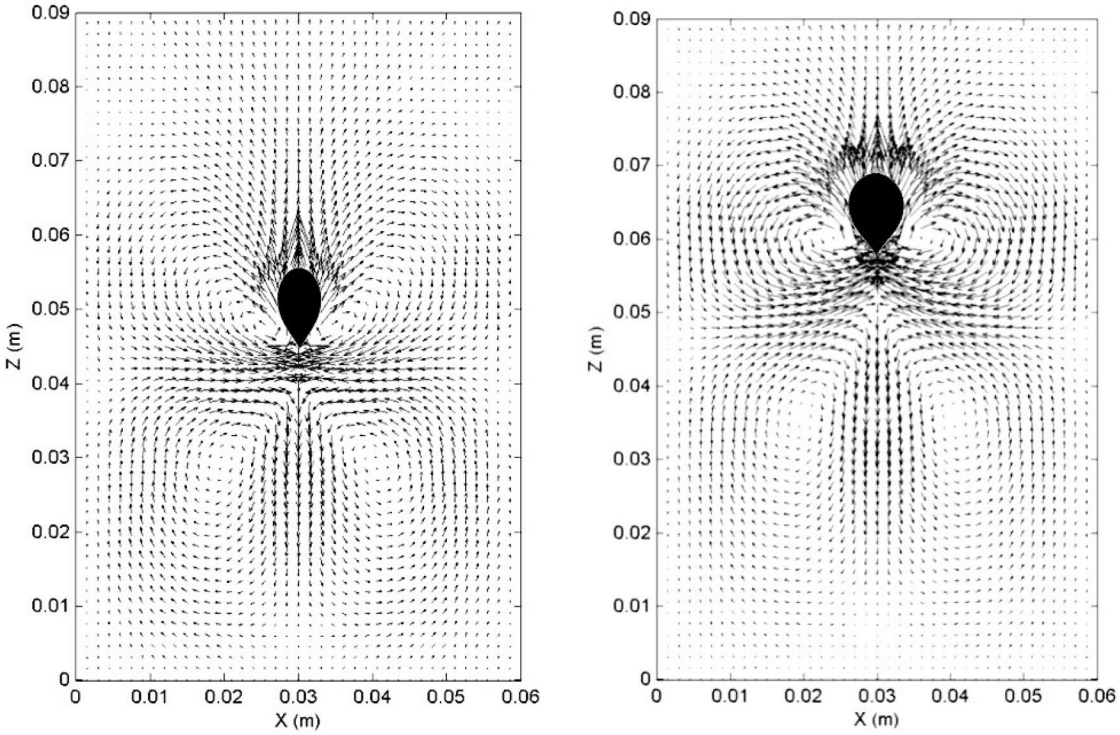

FIG. 5. Simulation results: flow field and bubble shape for a bubble rising in a 0.50% PAAm solution, on the left: bubble volume 80 mm^3; on the right: bubble volume 190 mm^3.

the negative wake, is also in good agreement with experiments (Fig. 2). Finally, our simulation produces correctly the teardrop shape of the bubble, even the emphasis was given to the computation of flow field.

Both the negative wake and bubble's teardrop shape predicted by the lattice Boltzmann approach are particularly noteworthy as they emerge naturally without special fitting within the LB scheme. In addition, a close analysis shows that the bubble's teardrop shape stems from a dual action of the negative wake drawing down the vertical axis of bubble and the lateral stresses stretching the bottom of the bubble, this phenomenon is experimentally confirmed. Obviously, this approach captures main features of the bubble rising in non-Newtonian fluid.

VI. CONCLUSION

In summary, we have developed a lattice Boltzmann scheme interfaced with a linear viscoelastic model that successfully captures the negative wake, the bubble's teardrop

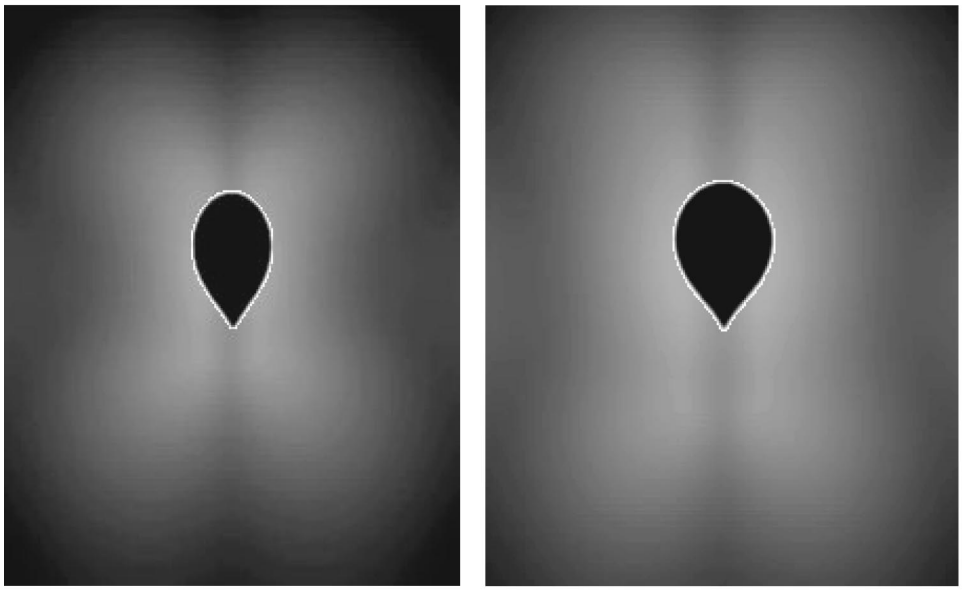

FIG. 6. Simulation results: simulated stress field around a bubble rising in a 0.50% PAAm solution, bubble volume on the left: 80 mm^3; on the right: 190 mm^3.

shape and the spatial stress distribution around the bubble rising in a non-Newtonian fluid. We are currently exploring the possibilities of complete measurements of largely extended flow field by PIV and 3D LB implementation. It is also envisaged that the present study could provide the basis for the further studies on long-range interactions and coalescence between bubbles through both velocity and stress fields as well as the bubble-fluid mass transfer.

[1] G. Astarita and G. Apuzzo, AIChE J. **11**, 815 (1965).
[2] G. F. Tiefenbruck and L. G. Leal, J. Non-Newtonian Fluid Mech. **7**, 257 (1980).
[3] O. Hassager, Nature (London) **279**, 402 (1979).
[4] H. Z. Li, Y. Mouline, L. Choplin, and N. Midoux, C. R. Acad. Sci., Ser. IIb: Mec., Phys., Chim., Astron. **324**, 491 (1997).
[5] H. Z. Li, X. Frank, D. Funfscilling, and Y. Mouline, Chem. Eng. Sci. **56**, 6419 (2001).
[6] S. Succi, *The Lattice Boltzmann Equation for Fluid Dynamics and Beyond* (Clarendon Press, Oxford, 2001).
[7] L. S. Luo and S. S. Girimaji, Phys. Rev. E **67**, 036302 (2003).
[8] N. Takada, M. Misawa, A. Tomiyama, and S. Fujiwara, Comput. Phys. Commun. **129**, 233 (2000).
[9] S. Chen and G. D. Doolen, Annu. Rev. Fluid Mech. **30**, 329 (1998).
[10] P. Lallemand, D. d'Humières, L. S. Luo, and R. Rubinstein, Phys. Rev. E **67**, 021203 (2003).
[11] I. Ispolatov and M. Grant, Phys. Rev. E **65**, 056704 (2002).
[12] A. J. Wagner, L. Giraud, and C. E. Scott, Comput. Phys. Commun. **129**, 227 (2000).
[13] D. Funfschilling and H. Z. Li, Chem. Eng. Sci. **56**, 1137 (2001).
[14] X. Frank, H. Z. Li, D. Funfscilling, F. Burdin, and Y. Ma, Can. J. Chem. **81**, 483 (2003).
[15] M. R. Swift, W. R. Osborn, and J. M. Yeomans, Phys. Rev. Lett. **75**, 830 (1995).
[16] M. R. Swift, E. Orlandini, W. R. Osborn, and J. M. Yeomans, Phys. Rev. E **54**, 5041 (1996).
[17] K. Langaas and J. M. Yeomans, Eur. Phys. J. B **15**, 133 (2000).